ACS OMEGA

http://pubs.acs.org/journal/acsodf

Mini-Review

Polymer Nanocomposites Containing Semiconductors as Advanced Materials for EMI Shielding

Kumari Sushmita, Giridhar Madras, and Suryasarathi Bose*

Cite This: *ACS Omega* 2020, 5, 4705−4718

Read Online

ACCESS | Metrics & More | Article Recommendations

ABSTRACT: Miniaturization of electronic devices and systems enhances the complexity of inbuilt circuitry, thereby giving rise to electromagnetic interference (EMI). EMI is a serious cause of concern as it affects the performance of a device, transmission channel, or system. In a quest to find an effective solution to this problem, several materials, apart from the conventional metals, such as carbon derivatives, have been extensively explored recently. In addition to carbon derivatives, hybrid structures such as core−shell, conjugated systems, etc. have also been researched. However, semiconducting fillers have received less attention, especially in this application. Hence, this review article will primarily focus on the systematic understanding of the use of semiconductor-based polymer nanocomposites and how the band gap plays a crucial role in deciding the dielectric properties and subsequently the electromagnetic absorption behavior for shielding applications. Our primary aim is to highlight the mechanism of shielding involved in such nanocomposites in addition to discussing the synthesis and properties that lead to effective shielding. Such nanocomposites containing semiconductors can pave the way for alternate materials for EMI shielding applications that are lightweight, flexible, and easy to integrate.

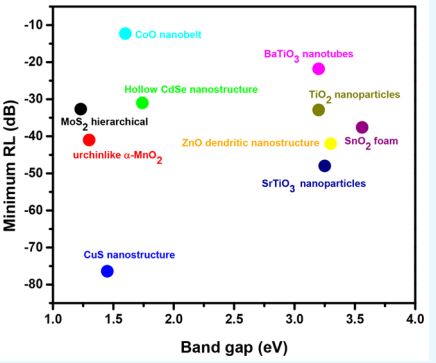

1. INTRODUCTION

The growing demand for electronic and communication devices in various sectors of military, industry, and commercial applications has led to a new kind of challenge called electromagnetic (EM) pollution. To combat this problem, the scientific and research community has initiated the development of various materials for electromagnetic interference (EMI) shielding applications, which range from metals to polymer nanocomposites. Polymer nanocomposite-based shield materials are advantageous over the conventional metal-based shield due to its low density, corrosion resistivity, ease of processability, and other applications. Once we step into the field of polymer nanocomposites, it spans a vast range of materials starting from various conducting and semiconducting fillers to a few insulating fillers. The conducting fillers that are commercially used include metal nanoparticles, carbon-based fillers such as graphene, carbon nanotubes (CNTs), carbon fibers (CFs), etc.[1] Mxene[2] comprises a newer class of conducting filler being investigated for EMI shielding. Mxenes are two-dimensional inorganic compounds, consisting of few-atom-thick layers of transition metal carbides, nitrides, or carbonitrides. The high conductivity of Mxenes has compelled the researchers to explore it for applications in the EMI shielding domain. There are several reviews explaining conducting fillers and its commercial usage. Herein, we will focus on the semiconducting fillers that are recently being explored among the research groups working in this field. The main reason behind stepping from conducting fillers toward semiconducting fillers is the various losses involved during the interaction of EM waves with matter at the GHz frequency range. The losses in this frequency range are not only attributed to ohmic, conduction, or eddy current losses but also to polarization losses, which might be a possible reason that compelled the scientific community to investigate the semiconducting fillers. However, the exact mechanism of shielding and various losses involved in the GHz frequency range is not well-established and is still under investigation. This review article will highlight the EMI shielding properties of semiconducting filler-based polymer nanocomposites, and to the best of our knowledge, no such review article has discussed this topic in detail.

A semiconductor is a material whose electrical conductivity value falls between a conductor and an insulator. The conventional semiconductors have a band gap between 1 and 1.5 eV, whereas wide band gap semiconductors have a band gap between 2 and 4 eV. It is to be noted that the value of the

Received: October 29, 2019
Accepted: February 25, 2020
Published: March 5, 2020

https://dx.doi.org/10.1021/acsomega.9b03641
ACS Omega 2020, 5, 4705−4718

band gap of a material is dependent on particle size[3] and also the phase of the material obtained. In this review article, we will cover semiconducting filler-based polymer nanocomposites with varying band gaps, as demonstrated in Table 1. The

Table 1. List of Semiconducting Materials That Can Be a Prospective Choice as Filler for EMI Shielding Applications

band gap (in eV)	materials	category
0.95−2	FeS_2,[4] Cu_2S,[5] CuO,[6] MoS_2,[7] MnO_2,[8] RuS_2,[4] CdSe,[9] OsS_2[4]	low band gap
1.3−2.5	CuS,[10] CoO,[11,12] WS_2,[13] Fe_2O_3,[14] Fe_3O_4,[15] CdS[16]	medium band gap
2−3.2	V_2O_5,[17] WO_3,[18] Cu_2O[6]	
3−4	MoO_3,[19] $BaTiO_3$,[20] TiO_2,[21] $SrTiO_3$,[22] ZnO,[3] ZnS,[23] SnO_2[24]	high band gap

various fillers in the table have been categorized as low, medium, and high band gap semiconductors for convenience. However, a few of the fillers mentioned in this list remain unexplored/less explored for EMI shielding applications. The primary aim of this work is to include literature that deals with a semiconducting filler in a polymer matrix, but due to lack of available data, a few papers that compared the shielding effectiveness data for the hybrid structures with control semiconducting fillers are also included in this review article. Semiconducting fillers such as $BaTiO_3$ and ZnO are very well studied along with their hybrid structures for EMI shielding applications, and hence only a few representative papers have been highlighted here. In each subsection of this article, composites with only a semiconducting filler will be covered first, followed by composites with hybrid fillers. Moreover, the focus of this work is also on the nonmagnetic semiconducting material as the magnetic fillers have been explored for EMI shielding applications in the recent past. It is also to be noted that this work focuses on polymer nanocomposites, and hence, literature involving non-polymer-based nanocomposites for EMI shielding applications are excluded, as is evident from the title of this work.

2. TERMINOLOGIES USED FOR EMI SHIELDING MEASUREMENTS

EM shielding is defined as the material's ability to attenuate EM radiations, and it is expressed either in terms of total shielding effectiveness (SE_T) or reflection loss/reflection coefficient (RL/RC).

SE_T is defined as the logarithm of the ratio of the incident power (P_I) to the transmitted power (P_T) and is calculated using eq 1.

$$SE_T = -10 \log \frac{P_I}{P_T} = SE_A + SE_R + SE_{MR} \quad (1)$$

where SE_A, SE_R, and SE_{MR} refer to the shielding via absorption, reflection, and multiple reflections, respectively.

SE_A, SE_R, and SE_{MR} can be represented by eqs 2, 3, and 4 respectively.

$$SE_A = -8.68d\sqrt{\frac{\omega\sigma\mu_r}{2}} \quad (2)$$

$$SE_R = -10 \log \frac{\sigma}{16\omega\varepsilon_0\mu_r} \quad (3)$$

$$SE_{MR} = 20 \log|(1 - 10^{-SE_A/10})| \quad (4)$$

where σ represents the total conductivity, ω is the angular frequency ($\omega = 2\pi f$), μ_r corresponds to the relative permeability of the shield material, d is the thickness of the shield, and ε_0 represents the dielectric constant in free space.

However, for magnetic metallic materials with dielectric loss and magnetic loss properties (ε and μ), shielding is generally defined in terms of reflection loss or reflection coefficient (RL or RC) and can usually can be evaluated by eq 5. So, a minimum RL signifies that the losses are mainly via the absorption mechanism.

$$\text{RL or RC} = 20 \log \frac{|Z_{in} - Z_0|}{|Z_{in} + Z_0|} \quad (5)$$

where Z_0 is the impedance of free space and Z_{in} is the input characteristic impedance and is defined as

$$Z_{in} = Z_0\sqrt{\frac{\mu_r}{\varepsilon_r}} \tanh\left\{j\left(\frac{2\pi fd}{c}\right)\sqrt{\mu_r\varepsilon_r}\right\} \quad (6)$$

where μ_r and ε_r are the relative permeability and relative permittivity of the shielding material, f is the frequency of incoming EM wave, d is the thickness of the shield material, and c is the velocity of light in a vacuum.

It is to be noted that few papers in the literature report the EMI shielding performance in terms of shielding effectiveness (SE_T, SE_A, SE_R), whereas others report it in terms of reflection loss or reflection coefficient (RL or RC). The correlation between SE and RL is difficult to obtain without the values of the relevant input parameters (as per eqs 1−6). It would have been easier to compare data if the results were expressed in terms of either SE or RL; however, given that many papers did not include both RL and shielding effectiveness data in the same paper, we reported the available data as is.

3. SEMICONDUCTING FILLER-BASED POLYMER NANOCOMPOSITES

3.1. Composites with Low Band Gap Fillers.

3.1.1. MoS_2-Based Composites. Transition metal dichalcogenides are 2D layered semiconductor materials of the type MX_2, with M as the transition metal (Mo, W, etc.) and X as the chalcogen (S, Se, or Te). MoS_2 is a well-known dichalcogenide used in photonics, photovoltaics, microelectronics, and hydrogen evolution applications. MoS_2 is one of the dichalcogenides gaining attention for EMI shielding applications. Zhang et al.[25] studied the MoS_2/polyvinylidene fluoride (PVDF) system for EMI shielding performance. It is observed that the minimum RL value of MoS_2/PVDF composites with a filler loading of 25 wt % reached −26.11 dB at 11.36 GHz for a thickness of 2.5 mm. In the 18−40 GHz frequency range, the minimum RL of −27.47 dB was observed at 18.47 GHz (for 30 wt % filler and 1.5 mm thickness) and of −32.67 dB was observed at 28.93 GHz (20 wt % filler and 3.5 mm thickness). Also, they observed that the MoS_2 hierarchical nanostructure showed a minimum RL value of −26.11 dB (at 11.36 GHz), which is much higher than that of bulk MoS_2/PVDF composites (−11.94 dB at ∼5.9 GHz) and micrometer-sized MoS_2/PVDF composites (−12.27 dB at ∼13.5 GHz) for 25 wt % filler loading and for a thickness of 2.5 mm. The authors claim that the microwave absorption mechanisms include various polarization, destructive interference theory, and multiple reflections. Menon et al.[26] measured the EMI shielding behavior

https://dx.doi.org/10.1021/acsomega.9b03641
ACS Omega 2020, 5, 4705−4718

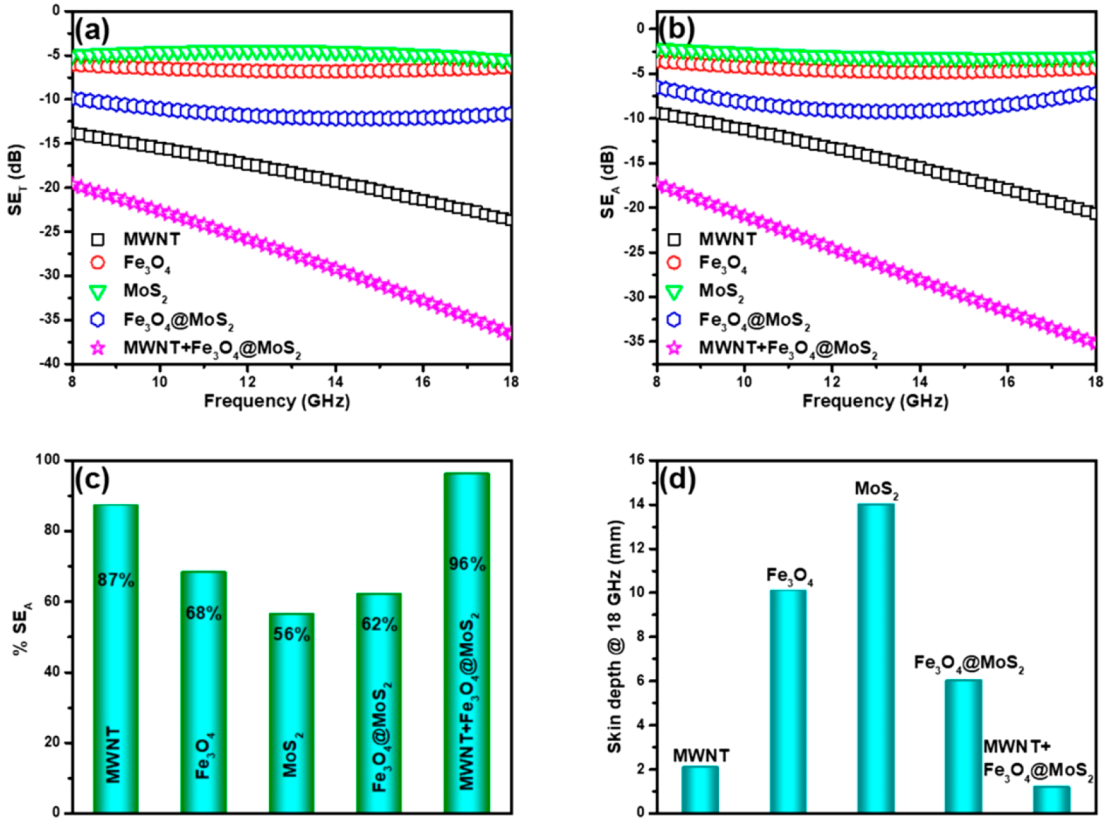

Figure 1. (a) Total shielding effectiveness, (b) shielding effectiveness due to absorption, (c) % shielding effectiveness due to absorption, and (d) skin depth of the composites. Reprinted from ref 26. Copyright 2019 American Chemical Society.

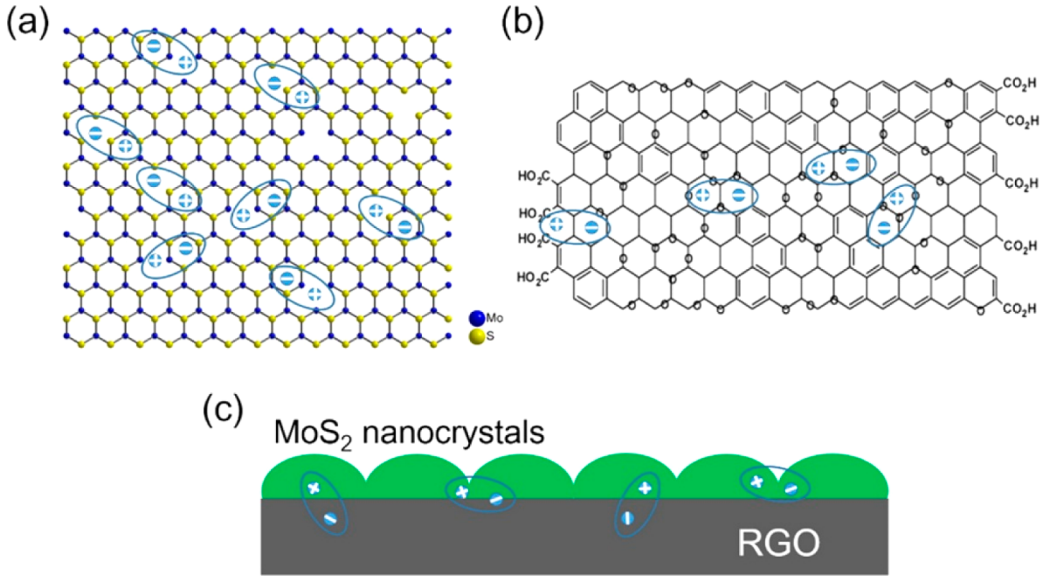

Figure 2. Schematic of dipole polarization in the MoS_2/rGO hybrid: (a) defect dipole polarization of MoS_2; (b) defect dipole polarization of rGO; (c) multiple interfacial polarizations in the MoS_2/rGO hybrid. Reprinted from ref 27. Copyright 2015 American Chemical Society.

(shown in Figure 1) of MoS_2, Fe_3O_4, Fe_3O_4@MoS_2, multiwalled carbon nanotube (MWCNT) and MWCNT/Fe_3O_4@MoS_2 in a dopamine-functionalized polyurethane (PU) matrix. The concentration of MWCNTs and other nanoparticles was fixed at 3 and 5 wt %, respectively, and the composite sample was made 5 mm thick. The total shielding effectiveness for 5 wt % MoS_2 is observed to be −5.5 dB, 5 wt % Fe_3O_4 is −6.3 dB, and 5 wt % Fe_3O_4@MoS_2 is −11.6 dB at 18 GHz frequency. However, the total shielding effectiveness increases as frequency increases for composite samples with MWCNTs. At 18 GHz, SE_T for a composite with 3 wt % MWCNT is observed to be −23.6 dB, and for the composite with 3 wt % MWCNT/5 wt % Fe_3O_4@MoS_2, it is observed to be −36.6 dB. The authors report shielding via absorption to be the primary cause of energy dissipation. They have attributed it to multiple internal reflections from MWCNTs, eddy current

https://dx.doi.org/10.1021/acsomega.9b03641
ACS Omega 2020, 5, 4705−4718

losses, interface polarization losses at the heterogeneous interfaces, and polarization losses from defect sites in the nanoparticles.

Wang et al.[27] studied the hybrids of MoS_2 and reduced graphene oxide (rGO) on microwave absorption performance. Both rGO and MoS_2 are semiconducting; however, the degree of reduction decides the band gap of rGO. With 10 wt % loading of the MoS_2/rGO in a wax matrix and for a sample thickness of 2.3 mm, the minimum RL of −50.9 dB was observed at 11.68 GHz frequency. They claimed that the microwave absorption is a result of three different mechanisms (shown in Figure 2): (a) the defect polarization of MoS_2 nanocrystals, (b) the defect polarization of the oxygen-containing groups and the imperfect carbon structures in rGO, and (c) the multiple interfacial polarization in MoS_2/rGO hybrids. Ding et al.[28] synthesized rGO-MoS_2 via hydrothermal synthesis and incorporated it in the paraffin matrix. They measured the EMI shielding performance of the composite and further compared it with pure MoS_2 and a pure rGO-based composite. With 10 wt % filler loading of rGO-MoS_2, the minimum RL value obtained was −41.53 dB at 11.36 GHz with a thickness of 3.0 mm. The proposed mechanism of shielding was similar to that mentioned by Wang et al.[27] Ran et al.[29] synthesized 3-methacryloxypropyltrimethoxysilane (KH570)-modified MoS_2 (M/MoS_2) and prepared a composite of the (M/MoS_2)/rGO nanosheet by embedding it in a PVP matrix. For a thickness of 3 mm, they obtained a minimum RL of −49.7 dB at 13.68 GHz with 18 wt % (M/MoS_2)/rGO. They have attributed the microwave absorption behavior to the defect dipole polarization as well as the multiple interfacial polarization.

3.1.2. MnO_2-Based Composites. Zhou et al.[30] synthesized hollow urchin-like α-MnO_2 nanostructures and studied the microwave absorption properties of α-MnO_2 nanostructures by mixing it with paraffin wax in a mass ratio of 1:1. The minimum RL of −41 dB was obtained at 8.7 GHz with a thickness of 1.9 mm. It is to be noted that, in general, MnO_2 nanostructures are antiferromagnetic materials, which implies that the magnetic loss is negligibly small and dielectric loss dominates the loss mechanism. The sample that exhibited minimum RL of −41 dB has lower tan δ_ε but higher tan δ_μ as compared to the sample in which MnO_2 was prepared under different experimental conditions. They further support their result by stating that it has been well-established in the literature that magnetic behavior can be disturbed by the dielectric behavior at a microwave frequency. Even with comparatively low tan δ_ε compared to that of the other sample, it has proved to be a better EM shield, and thus they claim that both dielectric and magnetic losses play a crucial role in this scenario. Moreover, they suggest that the microcircuit model explains the dielectric loss due to the inner walls of the urchin-like nanostructures, which can be considered as microloops, whereas actinomorphic one-dimensional MnO_2 can be considered as several antennas that convert electromagnetic waves into a vibrating microcurrent. This microcurrent can be produced in the microloops, leading to dielectric resonant peaks. Bora et al.[31] synthesized a PANI-α-MnO_2 nanorod composite and investigated the EMI shielding performance. With a thickness of 169 ± 2 μm, the composite showed most effective EMI SE_T of approximately −35 dB (EMI shielding due to absorption, SE_A ∼ −24 dB and EMI shielding due to reflection SE_R ∼ −11 dB) in the X-band, whereas SE_T was found to be approximately −39 dB (SE_A ∼ −29 dB and SE_R ∼ −10 dB) in the Ku-band. It is to be noted that α-MnO_2 is reported to be a better microwave absorber compared to other crystalline states. The EM shielding property of PANI-MnO_2 is attributed to the high dielectric loss incurred due to presence of MnO_2 and high electrical loss (dissipation current) that takes place along the PANI-grafted MnO_2 nanorods.

3.1.3. CdSe-Based Composites. Cao et al.[32] reported a ligand-assisted solvothermal synthesis of CdSe hollow nanostructures (70 wt %) and incorporated it in paraffin for EMI shielding applications. They also compared it with solid CdSe nanoparticles (70 wt %) in the paraffin matrix. It is observed that with 3 mm thickness and at 11.7 GHz frequency, minimum RL is −14 dB for CdSe hollow nanostructures, whereas the reflection loss for the solid CdSe nanostructures is more than −3 dB for frequencies above ∼11−18 GHz. For 4 mm thickness, two minima are observed in the value of RL (−16 dB at 5.6 GHz and −31 dB at 17.8 GHz). The authors claim that this difference in RL between the hollow and solid CdSe nanostructures has a size dependence. They explain that the size of the building blocks of CdSe nanostructures (small or large) decides the properties of the nanostructure, which further has its role in shielding. Moreover, both the real and imaginary parts of the relative permittivity for the hollow sample are higher than those for the solid one. This also indicates that the hollow CdSe nanostructures have an electrical conductivity higher than that of the solid ones, enhancing the microwave absorption properties.

3.2. Composites with Medium Band Gap Fillers.

3.2.1. CuS-Based Composites. He et al.[33] synthesized CuS nanostructures by varying the ratio of the precursors and observed that change in nanostructure resulted in the change in EMI shielding performance. For a shield thickness of 3.5 mm and CuS loading of 20 wt %, the minimum RL value for the CuS−paraffin composite is observed to be −76.4 dB at 12.64 GHz. The authors attribute the microwave absorption behavior to the CuS dielectric losses and interfacial polarization due to the heterogeneous structure of the composite. The flower-like CuS with a band gap of 1.45 eV was prepared by Hu et al.[34] using solvothermal synthesis. They prepared the EMI shielding samples by blending CuS with waterborne polyacrylate emulsion along with thickening agent and deionized water. Finally, this mixture was coated on a circular polytetrafluoroethylene (PTFE) plate to obtain a 0.6 mm thick EMI sample. SE_T was observed to be between −27 and −31 dB with CuS content as 28.6 wt % in the frequency of 300 kHz to 3 GHz. In another work by Hu et al.,[35] they explored PANI/flower-like CuS for EMI shielding performance. Compared to the original CuS and pure PANI, PANI/flower-like CuS composites exhibited enhanced SE_T. The EMI shielding was measured after incorporating PANI/CuS in the paraffin matrix. The optimal EMI SE_T of the PANI−CuS (50 wt % CuS) composites in paraffin reached −45.2 dB at 2.78 GHz for 3 mm thickness. It is to be noted here that the authors first prepared the PANI/CuS composite (20 wt %) and mixed it in the paraffin matrix. Also, an improved shielding efficiency (or shielding effectiveness) below −18 dB was obtained over the entire frequency range from 300 kHz to 3 GHz. The authors explained that the mobile charge carriers in CuS interacted with the electromagnetic fields. However, the enhanced EMI SE_T of the PANI−CuS composites is mainly attributed to the coordination bonding and the strong $\pi-\pi$ interactions between PANI and CuS. This may be useful for the charge transfer at the newly formed interface of PANI and CuS.

https://dx.doi.org/10.1021/acsomega.9b03641
ACS Omega 2020, 5, 4705−4718

Another reason that contributes to the SE_T is the flower-like structure CuS−PANI composites resulting in multiple scattering or reflections of incident EM radiations. Liu et al.[36] investigated CuS nanoflakes which were vertically aligned on magnetically decorated ($NiFe_2O_4$) graphene for EMI shielding performance. With 20 wt % magnetically decorated graphene/CuS in paraffin and for a thickness of 2.5 mm, the minimum RL was obtained to be −54.5 dB at 11.4 GHz frequency. CuS powder being a low band gap semiconductor is often used as an additive coating on the polymer surface to increase its conductivity. The author explains the mechanism of shielding by citing the free-electron theory. It says that an increase in conductivity of a composite could result in strong dielectric loss, and hence, they concluded that magnetically decorated graphene@CuS shows a stronger dielectric loss. They further explain that the magnetic loss is probably caused by natural resonance and an eddy current effect. While delving deeper into the mechanism, they add that CuS nanoflakes can also act as a microwave receiver, as the EM waves can get trapped in the inner voids and can lead to multiple reflections and scattering. They also suggest that the addition of magnetic particles in graphene sheets@CuS increases the microwave absorption properties due to better impedance matching, interfacial polarization, dipole polarization, and ion polarization. Also, the residual defects and groups in graphene sheets tend to introduce defect polarization relaxation, electron polarization, and relaxation processes that favor microwave absorption.

3.2.2. CoO-Based Composites. Sun et al.[37] studied the microwave absorption properties of CoO nanobelts and submicrometer CoO spheres. It was observed that the CoO nanobelts showed a strong broad peak at 14.2 GHz with a minimum RL of −12.3 dB, whereas the minimum RL reached −8.7 dB at 14.4 GHz for sub-micrometer spheres of CoO. It is to be noted that CoO nanostructures (70 wt %) were uniformly mixed in the paraffin matrix, and a shield of thickness 3 mm was obtained. CoO nanostructures are antiferromagnetic material, and thus there is negligible magnetic loss contribution. The major contribution to the microwave absorption is primarily due to the dielectric loss rather than the magnetic loss. The dielectric loss is known to originate from electronic polarization, ion polarization, and intrinsic electric dipole polarization, but it is the frequency range that decides which polarization is the dominant cause of the loss. The material crystal structure, size, and shape of nanomaterials influence the shielding properties as was observed in this paper,[37] where the change in the shape of CoO resulted in a change in shielding properties. From the electron microscopy characterization results, the authors concluded that the microwave-absorbing performance is associated with the single-crystal structure, the crystallization, and the aggregation degree of the nanocrystal building blocks.

3.2.3. WS_2-Based Composites. Zhang et al.[38] explored the microwave absorption property of WS_2-based composites. They synthesized WS_2−rGO by varying the mass ratios of GO (3, 4, 5, and 6%) and denoted the samples as S3, S4, S5, and S6. These samples were incorporated in 60% wax, and a shield with a thickness of ∼1.5 mm was prepared. SE_T of over −20 dB is obtained in the frequency range of 2−18 GHz, with a minimum of −32 dB for sample S5. The EMI shielding mechanism for WS_2−rGO architecture is explained in Figure 3. The dielectric loss and abundant multiscattering are the dominant reasons for energy dissipation. The dielectric loss

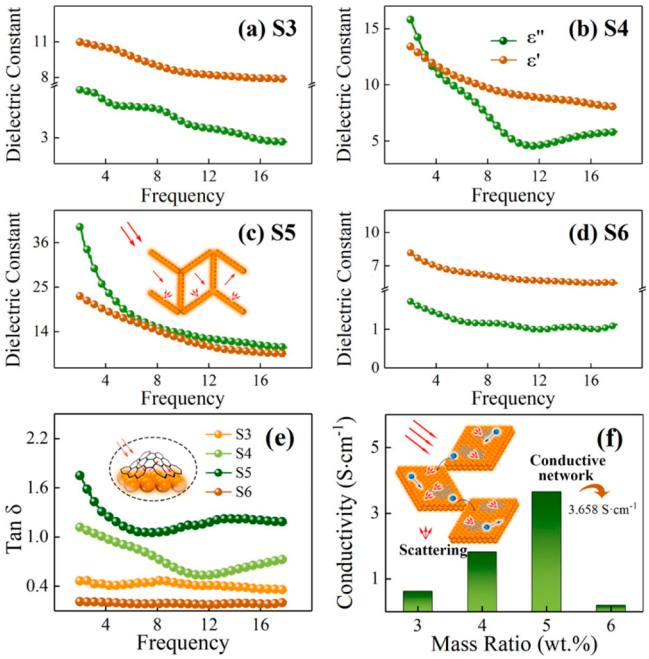

Figure 3. Real and imaginary permittivity plots of (a) S3 (mass ratio of GO/WS_2: 3), (b) S4 (mass ratio of GO/WS_2: 4), (c) S5 (mass ratio of GO/WS_2: 5), and (d) S6 (mass ratio of GO/WS_2: 6). (e) tan δ and (f) conductivity of WS_2−rGO architecture incorporated in wax (60%). The insets of (e,f) are the schematic for the interfacial polarization and electron transport paths in the WS_2−rGO architecture. Reprinted from ref 38. Copyright 2019 American Chemical Society.

comprises the conduction loss and relaxation loss. The difference in surface conductance between WS_2 and rGO results in an additional loss via the interfacial polarization which can be modeled as a capacitor. The literature for WS_2 is very limited, and dichalcogenides still remain an unexplored area for EMI shielding applications.

3.2.4. CdS-Based Composites. Lu et al.[39] studied the temperature-dependent microwave absorption properties of the CdS-MWCNT-based composite. They fabricated three kinds of structures, namely, MWCNTs coated with CdS nanocrystals (CdS-MWCNTs), coated with a thin CdS sheath (S-MWCNTs), and coated with a thick CdS sheath (TS-MWCNTs). For room-temperature tests, paraffin wax served the purpose of the matrix. The minimum RL of the wax matrix composite loading with CdS-MWCNTs is observed to be −25 dB (10 wt % filler loading and 3.5 mm thickness), which is 2.5 times higher than S-MWCNTs and 12 times higher than TS-MWCNTs. They attribute the strong absorption ability to the effective impedance matching in CdS-MWCNTs and dielectric loss. As per the Debye theory, ε'' denotes the dielectric loss, which comprises both polarizations and electrical conductivity originating from CdS-MWCNTs. The polarizations include the interfacial polarization due to abundant interfaces between CdS nanocrystals and MWCNTs and the dipolar polarization caused by surface functional groups, defects on/in acid-treated MWCNTs. Moreover, high aspect ratio and conductivity of MWCNTs and CdS-MWCNTs can build a conductive network in the composite for electron hopping and migration. In the case of S-MWCNTs and TS-MWCNTs, the CdS sheaths hinder the electron transfer between MWCNTs in the conductive network, which further decreases the dielectric loss.

https://dx.doi.org/10.1021/acsomega.9b03641
ACS Omega 2020, 5, 4705−4718

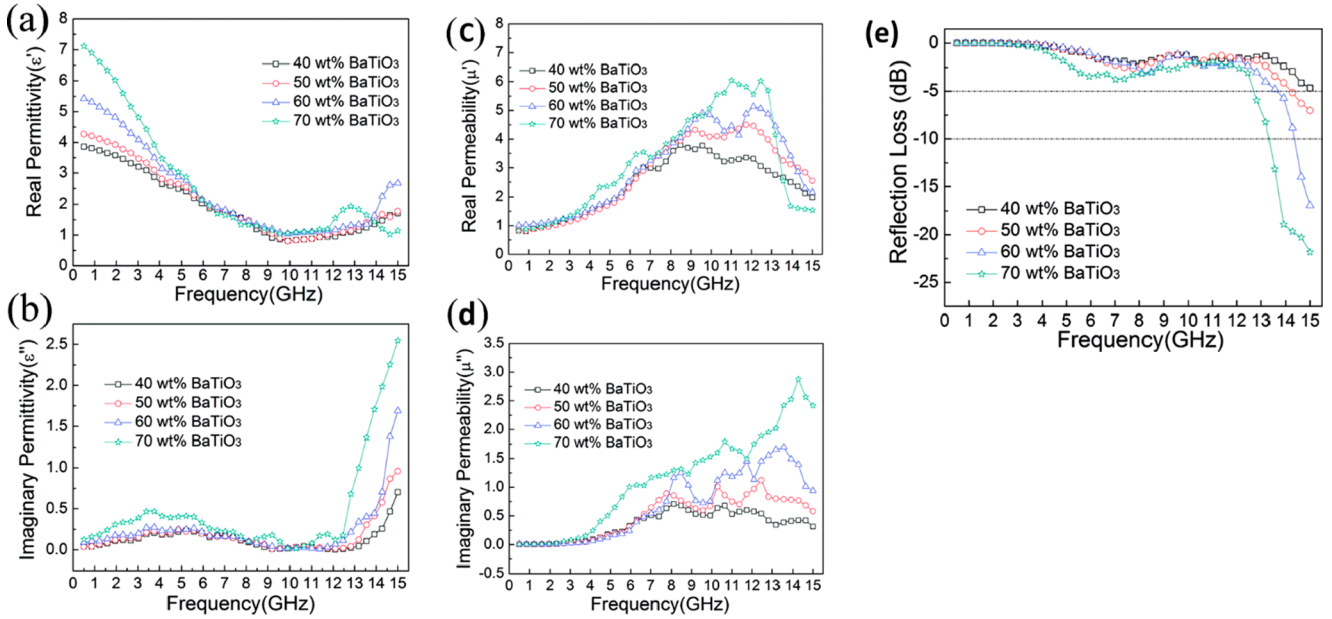

Figure 4. (a) Real permittivity, (b) imaginary permittivity, (c) real permeability, (d) imaginary permeability of the mixture of $BaTiO_3$ nanotubes and paraffin wax with different weight fraction, (e) RL for $BaTiO_3$−paraffin composite sample vs frequency for a sample thickness of 2 mm. Reprinted from ref 45. Copyright 2012 American Chemical Society.

3.2.5. WO_3-Based Composites. Sastry et al.[40] carried out an in situ polymerization of aniline monomer with camphor sulfonic acid (CSA) as dopant and ammonium persulfate as an oxidizing agent. They synthesized PANI-CSA tungsten oxide composites (PANI/CSA-WO_3) with a chemical oxidation method. With 40 wt % filler content, the obtained SE_T ∼ −13.8 dB at 14.2 GHz frequency. They claim that WO_3 acts as a lossy dielectric filler between the PANI/CSA chains, resulting in effective EM attenuation. Boujar Dolabi et al.[41] synthesized $WO_3/MnFe_2O_3$ nanoparticles (NPs core, 50/50 wt %) and via in situ polymerization obtained a core−shell structure of a $WO_3/MnFe_2O_3$/PANI nanocomposite (50 wt % as the core). With a thickness of 1.5 mm, a minimum RL of −12 dB was observed at 8.8 and 11.6 GHz. They attribute the shielding to the dielectric and magnetic losses. They further claim that the interfacial losses due to the changing boundary condition at various interfaces also contributes to the loss mechanism. Wang et al.[42] synthesized the hierarchical structure of graphene@Fe_3O_4@PANI@WO_3 (graphene@Fe_3O_4/WO_3 mass ratio = 2:1) and studied its microwave-absorbing performance after incorporating it in paraffin wax (70 wt % nanostructure). The EM wave absorption studies show that graphene@Fe_3O_4@PANI@WO_3 exhibits high EM wave absorption properties, with a minimum RL of −46.7 dB at 9.3 GHz for a thickness of 4 mm, which is higher than that of graphene@Fe_3O_4 (minimum RL = −15.4 dB at 14.1 GHz for a thickness of 1.5 mm) and graphene@Fe_3O_4@PANI (minimum RL = −20.9 dB at 9.4 GHz with a coating of 4 mm). The enhanced EM wave absorption mechanism of graphene@Fe_3O_4@PANI@WO_3 is ascribed to the improved impedance matching, enhanced interfacial polarization, and multiple scattering. Moreover, the presence of the PANI layer on the graphene sheet can lead to electron tunneling and enhanced electronic clouds, converting EM energy into heat. Herein, WO_3 particles in the hierarchical structure were designed to decrease permittivity, leading to an improvement in impedance matching.

3.3. Composites with High Band Gap Fillers.

3.3.1. MoO_3-Based Composites. Lyu et al.[43] synthesized $MoO_3/Mo_4O_{11}/MoO_2$ heterogeneous nanobelts (60 wt %) and incorporated them into the paraffin matrix. It showed a minimum RL of −59.2 dB at 10.8 GHz with a thickness of 4.6 mm. The EM absorption studies show that the high dielectric loss and enhancement in impedance matching due to the heterogeneous structure contribute to enhanced shielding. The heterogeneous interface leads to a formation of micro-capacitance and leads to enhancement in multiple scattering. Li et al.[44] synthesized 1D MoS_2/MoO_3 hybrids and incorporated them in the PVDF matrix. With a filler loading of 20 wt %, the minimum RL is found to be −38.5 dB at 8.7 GHz with a thickness of 1.9 mm. They attribute the shielding performance primarily to the dielectric losses. The uneven distribution of space charges between MoO_3 cores and MoS_2 shells leads to interfacial polarization, and the defects and residual groups in the low-crystalline MoS_2 shells can accumulate enough bound charges (dipoles) to generate considerable orientation polarization.

3.3.2. $BaTiO_3$-Based Composites. Zhu et al.[45] synthesized $BaTiO_3$ nanotubes via a wet chemical route. The dielectric loss at a lower frequency range (shown in Figure 4) is explained by the leak conductance, whereas relaxation polarization and electric conductance become dominant at a higher frequency range. The overall loss mechanisms in dielectric $BaTiO_3$ can be explained by dielectric polarization, spontaneous polarization, and the associated relaxation phenomena. Here, it becomes important to understand the difference between dielectric polarization and spontaneous polarization (a characteristic of ferroelectric material). Dipolar/dielectric polarization arises from molecules with a permanent electric dipole moment that can change orientation in an applied electric field. If a molecule of a substance has a permanent dipole moment, that is, they have a moment even in the absence of an electric field, it is called dipolar molecule and substances containing such molecules are called dipolar substance (for example, H_2O).

https://dx.doi.org/10.1021/acsomega.9b03641
ACS Omega 2020, 5, 4705−4718

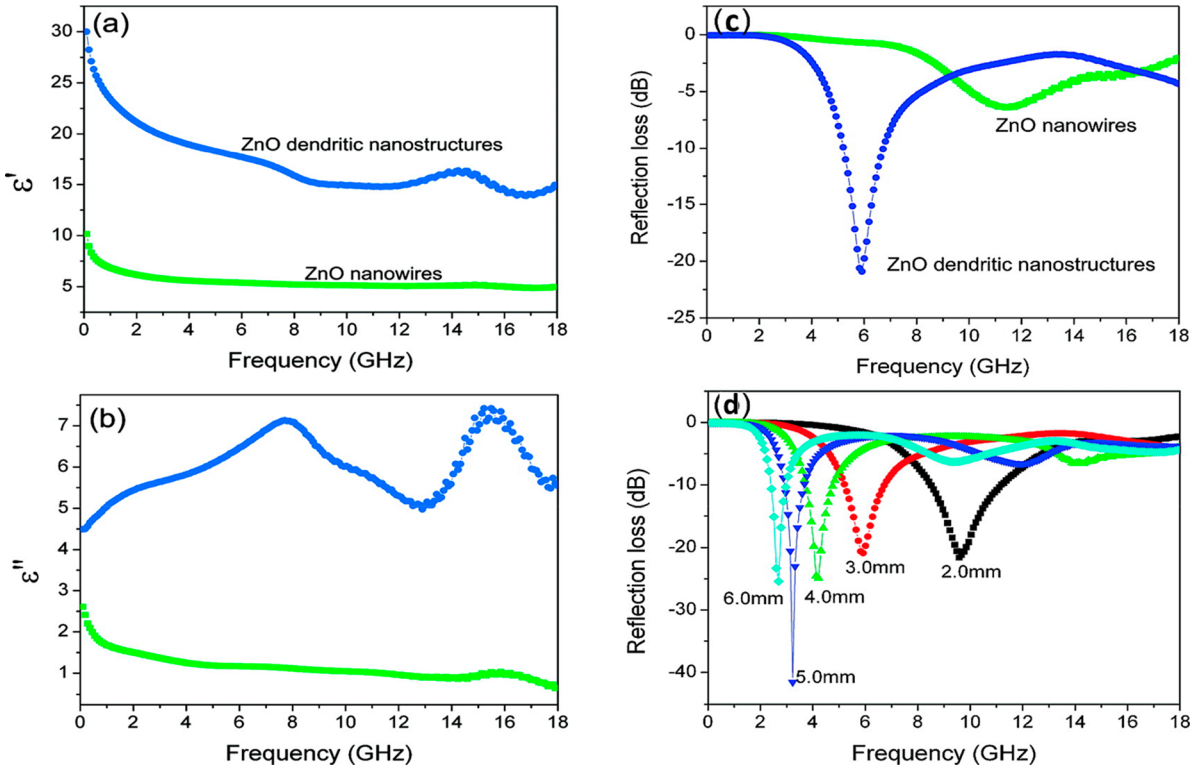

Figure 5. (a) Real and (b) imaginary parts of relative complex permittivity for a ZnO nanowire composite vs a dendritic nanostructured composite. (c) RL of 50 vol % ZnO nanowires vs 50 vol % ZnO dendritic nanostructure composites with a thickness of 3.0 mm. (d) RL of 50 vol % ZnO dendritic nanostructures composite with different thicknesses. Reprinted from ref 49. Copyright 2008 American Chemical Society.

It is to be noted that though the individual molecules in a dipolar substance have a permanent dipole moment, the net polarization disappears in the absence of an external electric field because the molecular moments are randomly oriented, resulting in complete cancellation of the polarization. However, $BaTiO_3$ is a ferroelectric crystal (a special class of dielectric material), and ferroelectrics exhibit an electric dipole moment even in the absence of an external electric field. Ferroelectrics generally consist of regions called domains. Within each of these domains, the polarization is in the same direction, but in adjacent domains, the polarization is in different directions. The net polarization depends on the difference in the volumes of the upward- and downward-directed domains. In the ferroelectric state, the center of the positive charge of the crystal does not coincide with the center of negative charge. They exhibit a spontaneous nonzero polarization even when the applied electric field is zero. This spontaneous polarization can be reversed by a strong applied electric field in the opposite direction. The polarization is therefore dependent not only on the current electric field but also on its history, yielding a hysteresis loop. It is worthwhile to note that crystal in a normal dielectric state usually does not show significant hysteresis with the electric field, but ferroelectrics do exhibit hysteresis. Ferroelectricity usually disappears above a certain temperature called the transition temperature.

The paper also shows the plots of μ' and μ'' (Figure 4c,d), which exhibits a resonance peak which may be related to natural resonance. However, as these values are higher than the ones reported in the literature, there could be a possibility of instrument error. In addition to this, the high interfacial area and hollow structure of nanotubes resulted in the minimum RL of −21.8 dB for $BaTiO_3$ nanotubes/paraffin wax composite at 15 GHz for a shield thickness of 2 mm and weight fraction of 70% (Figure 4e). Chauhan et al.[46] measured the EMI shielding performance of $BaTiO_3$-filled polyetherketone (PEK) composites in the X-band. Total shielding effectiveness of −11 dB (∼92% attenuation) is observed for a shield thickness of 2 mm and filler content of 18 vol %. As the dielectric loss due to $BaTiO_3$ is the major cause of EM attenuation, the author attributes the loss to the polarization effect. Abbas et al.[47] studied the complex permittivity and RL of $BaTiO_3$/polyaniline in the polyurethane matrix for X-band frequencies. Composite samples were prepared by dispersing $BaTiO_3$/PANI particulates in a two-pack polyurethane matrix that consisted of polyol-8 and hexamethylene diisocyanate mixed in 50:50 ratios. A minimum RL of −15 dB was observed for a sample ($BaTiO_3$/polyaniline = 1:3) with a thickness of less than 3.0 mm at 10 GHz frequency. $BaTiO_3$ is a ferroelectric material exhibiting high resistivity. Ba^{2+} and O^{2-} ions form a face-centered cubic lattice, with Ti^{4+} ions fitting in the octahedral interstices. At room temperature, the Ti^{4+} ions are possibly at minimum energy, which is off-centered and thus gives rise to permanent electric dipoles. When protonated by HCl acid solution, polyaniline also possesses permanent electric dipoles. Thus, dipolar polarization becomes one of the contributing factors in the loss mechanisms, owing to the dielectric nature of filler and matrix. Joule heating due to inherent conductivity of the polyaniline adds to the loss mechanism. Interfacial polarization is also expected due the heterogeneous structure of the composite.

Guo et al.[48] also studied the $BaTiO_3$-based composite for EMI shielding applications. The composite with 15 wt % rGO@$BaTiO_3$ in the PVDF matrix showed the minimum RC

https://dx.doi.org/10.1021/acsomega.9b03641
ACS Omega 2020, 5, 4705−4718

of −45.3 dB at 5.44 GHz for a thickness of 4.5 mm. They also calculated the SE_T and found that 30 wt % filler demonstrates a minimum SE_T of up to −9.8 dB in the frequency range of 2−14 GHz.

3.3.3. TiO_2- and ZnO-Based Composites. Zhuo et al.[49] synthesized dendritic nanostructures by a two-step chemical vapor deposition process and compared the results of dielectric and microwave shielding properties with ZnO nanowires. Figure 5 shows the complex permittivity and RL plot of the primary ZnO nanowires composite versus the ZnO dendritic nanostructured composite. The filler content was 50 vol % in a paraffin matrix. The real permittivity of the ZnO nanowire composite is observed to be nearly 5.0, and the imaginary permittivity is about 1.0. However, the real part of relative permittivity showed a decrease from 30 to 15 as the frequency increases for ZnO dendritic nanostructures. It exhibits a peak in the frequency range of 13−17 GHz. The imaginary part of permittivity shows an increase from 4 to 7, and the curve exhibits two broad peaks in the frequency range of 0.1−13 and 13−17 GHz. This resonance behavior is expected for a highly conductive composite with significant skin effect. The response of ZnO nanostructures can be attributed to the electronic spin and charge polarization due to polarized centers. The value of the minimum RL for the ZnO dendritic nanostructure composite is −42 dB at 3.6 GHz with a thickness of 5.0 mm. Excellent dielectric and microwave shielding properties are observed for complicated interfaces of ZnO dendritic nanostructures compared to nanowires, and thus it can be concluded that morphology has a significant role in microwave absorption.

Singh et al.[50] studied the EMI shielding behavior of nanocomposites based on transition metal oxides in poly(vinyl alcohol) (PVA). They studied different transition metal oxides such as Fe_2O_3, ZnO, SiO_2, ZrO_2, and TiO_2 incorporated in the PVA matrix in the frequency range of 4−8 GHz (C-band) and 8−12 GHz (X-band). At 10 wt % concentration level and 0.5 mm thickness, the minimum reflection loss values for the composites containing Fe_2O_3, ZnO, SiO_2, ZrO_2, and TiO_2 were found to be −38.85 (10.4 GHz), −33.65 (10.4 GHz), −41.90 (10.4 GHz), −24.90 (11.0 GHz), and −32.90 dB (9.76 GHz), respectively. PVA is not 100% transparent to EM radiations, and thus it also shows a minimum reflection loss of −21.50 dB at 10.4 GHz frequency. It is to be noted here that Fe_2O_3, ZnO, and TiO_2 are the semiconducting oxides, whereas ZrO_2 and SiO_2 have a band gap greater than 5 eV. The authors have attributed the losses in SiO_2-, ZnO-, ZrO_2-, and TiO_2-based nanocomposites to be dielectric in nature, whereas they claim that Fe_2O_3-based nanocomposites exhibit both dielectric and magnetic losses.

Phang et al.[51] synthesized hexanoic acid (HA)-doped PANI nanocomposites containing TiO_2. Pani/HA/TiO_2 nanocomposite with the highest permittivity, heterogeneity, and loss tangent showed a minimum RL of −31 dB at 10 GHz. Dhawan et al.[52] synthesized a conducting ferrimagnetic polyaniline nanocomposite with γ-Fe_2O_3 (9−12 nm) and TiO_2 (70−90 nm) nanoparticles. A different formulation of polymer nanocomposite having an aniline/TiO_2/γ-Fe_2O_3 weight ratio of 1:1:1 (PTF11) and 1:1:2 (PTF12) was chosen along with composite having aniline/TiO_2 weight ratio of 1:1 and aniline/γ-Fe_2O_3 (PF12) weight ratio of 1:2 for comparison. The polyaniline−TiO_2−γ-Fe_2O_3 nanocomposite showed enhanced shielding effectiveness (SE_A ∼ −45 dB) compared to that of polyaniline−γ-Fe_2O_3 (SE_A ∼ −8.8 dB) and polyaniline−TiO_2 (SE_A ∼ −22.4 dB) nanocomposite for the frequency range of 12.4−18 GHz (Ku-band). Losses due to TiO_2 is a result of its high dielectric constant along with strong dipolar polarization and the associated relaxation phenomenon. γ-Fe_2O_3 and TiO_2 in the polyaniline matrix leads to a significant increase in a real and imaginary part of complex permittivity. It can be attributed to the interfacial polarization due to the presence of insulating γ-Fe_2O_3 particles and high dielectric TiO_2 particles. Absorption-based EMI shielding is mainly attributed to the combined effect of magnetic and dielectric losses incurred due to the incorporation of γ-Fe_2O_3 and TiO_2. In another work by Akman et al.,[53] they exploited the combined effect of $BaFe_{12}O_{19}$ and TiO_2 on EMI shielding performance. They varied the weight fractions of $BaFe_{12}O_{19}$/TiO_2 weight fractions and compared the nanocomposites with and without polypyrrole (Ppy) coating. The dielectric loss saw a significant jump in the samples with Ppy coating in the frequency range of 8−18 GHz. The sample having an equal amount of magnetic and dielectric fillers and with Ppy coating showed a minimum RL of −35 dB at 16.5 GHz. However, the minimum RL of −45 dB at 17.5 GHz was obtained for the sample with a higher amount of magnetic filler and without Ppy coating.

Kong et al.[54] gave a good insight into the EM-absorbing material and its need to have a suitable permittivity and dielectric loss value. With the increase in dielectric loss, the absorption coefficient increases, but the problem arises because, as the dielectric loss is enhanced, the permittivity also increases and subsequently the EM reflection increases. This poses a problem as the aim of a good shield is to enhance the EM absorption capabilities. It is revealed that the materials having high EM absorption capability require a low real part of permittivity and an appropriately high electrical conductivity (around 1 S/m). Alternatively, when the permittivity meets the EM impedance match requirement, higher dielectric loss implies better EM absorption properties. It is to be noted that the electrical conductivity is related to the imaginary part of permittivity (ε'') according to eq 7.

$$\sigma = 2\pi f \varepsilon_0 \varepsilon'' \tag{7}$$

Here, σ represents the electrical conductivity (S/m), ε_0 is the permittivity of free space, and f is the frequency (Hz). From the above description, it is also evident that the value of 1 S/m required for good EM absorption ability lies in the semiconducting range. Moreover, they have also presented a chart, as shown in Figure 6, which relates the real and imaginary part

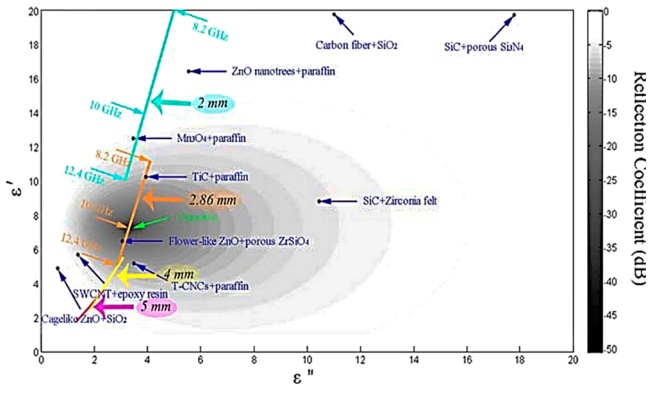

Figure 6. Chart relating different material with permittivity and reflection coefficient. Reprinted from re 54. Copyright 2013 American Chemical Society.

https://dx.doi.org/10.1021/acsomega.9b03641
ACS Omega 2020, 5, 4705−4718

Table 2. List of Semiconducting Materials That Can Be a Prospective Choice as Filler for EMI Shielding Applications

Sl. no.	filler	matrix	SE_T/minimum RL	thickness (mm)	frequency	ref
1	(a) MoS_2 hierarchical structure (25 wt %)	PVDF	RL= −26.11 dB	2.5	11.36 GHz	25
	(b) bulk MoS_2		RL= −11.94 dB		∼5.9 GHz	
	(c) micrometer-sized MoS_2		RL= −12.27 dB		∼13.5 GHz	
2	MoS_2 hierarchical structure (30 wt %)	PVDF	RL = −27.47 dB	1.5	18.47 GHz	25
3	MoS_2 hierarchical structure (20 wt %)	PVDF	RL = −32.67 dB	3.5	28.93 GHz	25
4	MoS_2 (5 wt %)	dopamine-functionalized PU	SE_T = −5.5 dB	5	18 GHz	26
5	Fe_3O_4 (5 wt %)	dopamine-functionalized PU	SE_T = −6.3 dB	5	18 GHz	26
6	Fe_3O_4@MoS_2 (5 wt %)	dopamine-functionalized PU	SE_T = −11.6 dB	5	18 GHz	26
7	3 wt % MWCNT/5 wt % Fe_3O_4@MoS_2	dopamine-functionalized PU	SE_T = −36.6 dB	5	18 GHz	26
8	MoS_2/rGO (10 wt %)	wax	RL = −50.9 dB	2.3	11.7 GHz	27
9	MoS_2/rGO (10 wt %)	paraffin	RL = −41.53 dB	3	11.7 GHz	28
10	(M/MoS_2)/rGO (18 wt %)	PVP	RL = −49.7 dB	3	13.7 GHz	29
11	α-MnO_2 (α-MnO_2/paraffin = 1:1 (mass ratio))	paraffin	RL = −41 dB	1.9	8.7 GHz	30
12	α-MnO_2	PANI	SE_T = −35−39 dB	∼0.169	8.2−18 GHz	31
13	hollow CdSe nanostructure (70 wt %)	paraffin	RL = −31 dB	4	17.8 GHz	32
14	CuS nanostructure (20 wt %)	paraffin	RL = −76.4 dB	3.5	12.64 GHz	33
15	CuS (28.6 wt %)	PA/PTFE	SE_T = −27−31 dB	0.6	300 kHz to 3 GHz	34
16	PANI/CuS (50 wt % CuS), 20 wt % PANI/CuS	paraffin	SE_T = −45.2 dB	3	2.8 GHz	35
17	CuS/$NiFe_2O_4$/graphene (20 wt %)	paraffin	RL = −54.5 dB	2.5	11.4 GHz	36
18	CoO nanobelt (70 wt %)	paraffin	RL = −12.3 dB	3	14.2 GHz	37
19	CoO microsphere (70 wt %)	paraffin	RL = −8.7 dB	3	14.4 GHz	37
20	WS_2/rGO (40 wt %)	wax	SE_T = −20 to −32 dB	∼1.5	2−18 GHz	38
21	Fe_2O_3 (10 wt %)	PVA	RL = −38.85 dB	0.5	10.4 GHz	50
22	CdS-MWCNTs (10 wt %)	paraffin wax	RL = −25 dB	3.5	8−9 GHz	39
23	WO_3 (40 wt %)	PANI/CSA	SE_T ∼ −13.8 dB		14.2 GHz	40
24	WO_3/$MnFe_2O_3$ (50/50 wt %) (50 wt % as core)	PANI (as shell)	RL = −12 dB	1.5	8.8 and 11.6 GHz	41
25	graphene@Fe_3O_4@PANI@WO_3 (70 wt %) (mass ratio of graphene@Fe_3O_4/WO_3 = 2:1)	paraffin	RL = −46.7 dB	4	9.3 GHz	42
26	MoO_3/Mo_4O_{11}/MoO_2 (60 wt %)	paraffin	RL = −59.2 dB	4.6	10.8 GHz	43
27	1D MoS_2/MoO_3 (20 wt %)	PVDF	RL = −38.5 dB	1.9	8.7 GHz	44
28	$BaTiO_3$ nanotubes (70 wt %)	paraffin	RL = −21.8 dB	2	15 GHz	45
29	$BaTiO_3$	PEK	SE_T = −11 dB	2	8.2−12.4 GHz	46
30	($BaTiO_3$/polyaniline = 1:3)	PU	RL = −15 dB	∼ 3	10 GHz	47
31	rGO@$BaTiO_3$ (wt % mentioned in RL/SE_T column)	PVDF	RL = −45.3 dB (15 wt %), SE_T = −9.8 dB (30 wt %)	4.5	5.4 GHz (for RL), 10 GHz (for SE_T)	48
32	ZnO dendritic nanostructure (50 vol %)	paraffin	RL = −42 dB	5	3.6 GHz	49
33	TiO_2 (10 wt %)	PVA	RL = −32.90 dB	0.5	9.8 GHz	50
34	ZnO (10 wt %)	PVA	RL = −33.65 dB	0.5	10.4 GHz	50
35	TiO_2	Pani/HA	RL = −31 dB		10 GHz	51
36	TiO_2/γ-Fe_2O_3	Pani	SE_A = −45 dB		∼14.5 GHz	52
37	$BaFe_{12}O_{19}$/TiO_2 (1:1)	polypyrrole	RL = −45 dB	2	17.5 GHz	53
38	ZnO/$ZnAl_2O_4$ (40 wt %)	paraffin	RL/RC = −25 dB	2.86	9.7 GHz	54
39	ZnO/MWCNT (40 wt %)	wax	RL = −36 dB	5	5−6 GHz	55
40	C/ZnO (40 wt %)	paraffin wax	RL/RC = −52 dB	1.75	11 GHz	56
41	rGO/ZnO (10 wt %)	paraffin	RL = −25.31 dB	3	11.5 GHz	57
42	$SrTiO_3$ (50 wt %)	epoxy	RL = −48 dB	1	14.5 GHz	58
43	$SrTiO_3$ (0.3 volume fraction)	epoxy	RL = −34 dB	5	4.3 GHz	59
44	SnO_2 NWs (20 vol %)	paraffin	RL = −32.5 dB	5	14 GHz	60
45	SnO_2 foam (30 wt %)	paraffin wax	RL = −37.6 dB	2	17.1 GHz	61
46	Fe_3O_4@SnO_2 (Fe_3O_4@SnO_2/epoxy = 1:5 by mass)	epoxy	RL = −36.5 dB	2	7 GHz	62

of permittivity with RC/RL (calculated from eq 5). The minimum value of RC is a function of frequency and thickness (shown in Figure 6). The four-color lines in Figure 6 signify that the permittivity corresponding to a minimum RC decreases with the increase of thickness and frequency. The blue color line represents the minimum RC corresponding to 2

https://dx.doi.org/10.1021/acsomega.9b03641
ACS Omega 2020, 5, 4705−4718

mm thickness. It is observed that the complex permittivity of the minimum RC is reduced from 20−5*j* to 10−3*j* when the frequency changes from 8.2 to 12.4 GHz. Orange, yellow, and red lines represent thicknesses of 2.86, 4, and 5 mm, respectively. Also, the paper claims that no material in literature satisfies the condition of optimum combination of the real and imaginary parts of permittivity to serve the dual purpose of RC and maximizing effective absorption bandwidth. Hence, to improve absorption properties and to obtain optimal permittivity, it is desired to design materials with special composition and microstructure. In their work, they have synthesized $ZnO/ZnAl_2O_4$ composite powders via sol−gel synthesis. Sub-micrometer-sized ZnO acts as an electrically lossy phase, and $ZnAl_2O_4$ nanograins act as a medium permittivity phase. $ZnO/ZnAl_2O_4$ (40 wt %), when incorporated in the paraffin matrix, exhibits appropriate permittivity and electrical conductivity, which can be attributed to the high carrier concentration and mobility at the interfaces. For a sample thickness of 2.86 mm, the minimum RC reaches −25 dB (whole X-band) for the sample with $ZnO/ZnAl_2O_4$ in the molar ratio of 88.9:11.1.

In another work by Song et al.,[55] they decorated ZnO particles on MWCNTs and incorporated them in wax. With 40 wt % ZnO/MWCNT content in the wax, the minimum RL was obtained as −36 dB for a 5 mm thick shield between 5 and 6 GHz. They described shielding behavior using a resistor−capacitor model. They claim that the MWCNT/ZnO shows resonant absorption, which implies two different types of RL peaks caused by the quarter-wavelength attenuation and the MWCNT/ZnO interface. Han et al.[56] studied C/ZnO nanoparticles mixed in paraffin wax for electromagnetic shielding performance. With 40 wt % nanofillers, the composite shows a minimum RC of −52 dB at 11 GHz with a sample thickness of 1.75 mm. Compared to pure carbon spheres and ZnO hollow spheres, the core/shell structure of C/ZnO composites showed promising results with high dielectric loss and moderate impedance match. In a work by Wu et al.,[57] they synthesized 3D rGO/ZnO nanoparticles followed by subsequent UV irradiation to remove the remnant oxygen functional groups from rGO. They incorporated these nanoparticles in the paraffin matrix (10 wt %). It was observed that, for a sample thickness of 3 mm, the minimum RL is −25.31 dB at 11.52 GHz.

3.3.4. $SrTiO_3$-Based Composites. Murugan et al.[58] hydrothermally synthesized cubic $SrTiO_3$ nanoparticles and made them into a composite with epoxy as a polymer matrix. With a filler content of 50 wt % and a shield thickness of 1 mm, the composite exhibited a minimum RL of −48 dB at 14.5 GHz frequency. $SrTiO_3$ in an epoxy matrix was also studied by Choi et al.[59] It is observed that the minimum RL for a 5 mm thick composite with 0.6 volume fraction of $SrTiO_3$ is −30 dB at 9 GHz, and the composite containing a 0.3 volume fraction of $SrTiO_3$ shows a minimum RL of −34 dB at 4.3 GHz. The authors have plotted the complex permittivity and permeability with an increase in frequency, and it is evident that the dielectric losses are one of the dominant factors resulting in EMI shielding performance.

3.3.5. SnO_2-Based Composites. Feng et al.[60] studied the effect of SnO_2 nanowires (NWs) on the EMI shielding performance. The value of minimum RL for the composites with 20 vol % SnO_2 NWs were found to be approximately −32.5 dB at 14 GHz with a thickness of 5.0 mm. They observe that microwave absorption exhibited by the composite is due to the dielectric loss rather than magnetic loss. The authors propose that dipolar polarization and the associated relaxation phenomena of SnO_2 constitute the loss mechanisms. It has been studied that composite materials, in which semiconductor NWs are coated with a dielectric nanolayer, introduce additional interfaces and more polarization charges at the surface. The interfacial polarization and the associated relaxation in such cases add to the loss mechanism. Further, they have suggested that the molecular dipoles formed at the NWs' surface interact with the microwave field, resulting in some absorption losses through heating. Zhao et al.[61] synthesized honeycomb-like SnO_2 foams via the polystyrene template method. The SnO_2 foams were uniformly blended with paraffin wax at 30% weight fraction, and EMI shielding measurements were done for 2 mm thick samples. The minimum RL is reported to be −37.6 dB at 17.1 GHz, with RL below −10 dB at 5.6 GHz (12.4−18.0 GHz). The enhanced microwave absorption properties were ascribed to dipole polarization. The small SnO_2 nanoparticles serve the purpose of dipoles in the SnO_2 foam. Interfacial polarization, impedance match, multiple reflection, and diffuse scattering further adds to the mechanism of shielding. Liu et al.[62] synthesized an Fe_3O_4@SnO_2 yolk−double-shelled structure with a magnetic Fe_3O_4 core and a dielectric SnO_2 as a double shell. The composite samples were prepared by mixing the Fe_3O_4@SnO_2 and epoxy resin in a mass ratio of 1:5. The RL for the double-shelled Fe_3O_4@SnO_2 yolk−shell microspheres reached a minimum of −36.5 dB at 7 GHz with a shield thickness of 2 mm. The authors suggest that the shielding is due to the absorption losses arising out of the interaction of EM waves with the shield material. It is not only the dielectric losses due to SnO_2 and the magnetic losses due to the Fe_3O_4 playing role but also the synergistic effect of SnO_2 and Fe_3O_4. The dielectric constant and loss increase due to effective interfaces between the dielectric and magnetic materials, thus resulting in loss via interfacial polarization. However, the authors suggest that the void spaces and high porosity of the yolk−shell microspheres might also act as active sites for internal scattering of EM waves.

4. SUMMARY OF SEMICONDUCTING FILLERS USED IN POLYMERIC SHIELDS

Table 2 discusses the summary of the literature discussed in this article. It is quite difficult to compare different semiconducting materials as the parameter for measurement varies in each paper. So, we cannot exactly conclude the role of the band gap of filler material for EMI shielding applications. However, this table gives a preliminary idea as to how different semiconducting fillers perform in the area of microwave absorption via dielectric, interfacial, and scattering losses.

As most of the semiconducting fillers stated above exhibit dielectric losses as one of their primary mechanism of shielding, it is worthwhile to study the relation between semiconducting nature and dielectric behavior of a material. We carried out a literature survey to figure out if there exists any relationship between the band gap and dielectric properties. Yim et al.[63] confirmed that, for most of the oxides, there is an inverse correlation between the band gap and the real part of permittivity. They compiled the result of well-known oxides in Figure 7. However, they also mentioned that there do exist certain materials that show large permittivity, despite their large band gaps.

https://dx.doi.org/10.1021/acsomega.9b03641
ACS Omega 2020, 5, 4705−4718

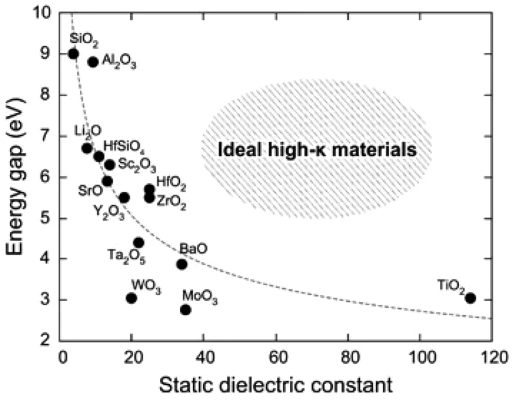

Figure 7. Experimental band gap and dielectric constant for well-known oxides. Reprinted with permission from ref 63. Copyright 2015 Springer Nature.

However, in EMI shielding applications, it is the trend of dielectric loss and tan δ that is a primary concern as our focus lies in lossy materials. Dielectric constant, dielectric loss, and tan δ of each material are all size-dependent and frequency-dependent functions. Thus, it becomes complicated to find a universal law that suits each material and for all frequencies. However, studies have been done to understand the underlying principles. Sun et al.[64] studied the dielectric suppression and their dependence on band gap for nanometric semiconductors. The complex dielectric constant was correlated to the band gap, which has a dependence on the crystal field. The crystal field was further found to be a function of atomic separation and charge transportation. They have also plotted a graph showing energy dependence of the suppression of ε'' of the nanometric semiconductors with respect to the direct and indirect band gap transitions. It is observed that $(\Delta\varepsilon_r''/\varepsilon_r')$ increases as $(\hbar\omega/E_g)$ increases. Sati et al.[65] studied the variation of dielectric constant and dielectric loss at 5 MHz frequency as a function of Hf doping in $BaTiO_3$. They showed that with an increase in Hf doping in $BaTiO_3$, the band gap increases and the value of the dielectric constant and that of dielectric loss/tan δ systematically decrease. They have also stated that it is well-studied that Hf doping at the Ti site reduces tetragonality, which probably leads to the decrease in the value of dielectric constant. They also mentioned that Penn theoretically derived the dielectric constant (ε') of semiconductors in terms of plasma frequency (ω_p) and optical band gap (E_g) as[65]

$$\varepsilon'(0) \sim 1 + (h\omega_p/E_g)^2 \quad (8)$$

As per the Drude's theory, ω_p is defined as $(ne^2/m_e\varepsilon_0)^{0.5}$, where n is the number density of electrons, e is the electric charge, m_e is the effective mass of the electron, and ε_0 is the permittivity of free space.[66]

For an insulating/semiconducting system, the dielectric loss, that is, leakage current, is related to band gap according to the following equation:[65]

$$\sigma = \sigma_0 \exp\left(-\frac{E_g}{2KT}\right) \text{(for intrinsic case, } E_a = E_g/2) \quad (9)$$

Equation 9 implies that, with an increase in the band gap, the conductivity should decrease. In their work, they further proposed that increasing the value of E_g leads to a decrease in the tunneling probability of electron from the valence band to the conduction band, which resulted in the lowering of dielectric loss.

Hence, the general rule of thumb implies that, with the increase in the band gap, the dielectric constant decreases (as shown in Figure 7 and eq 8).[54,63,65] The same trend is followed by dielectric loss. As the band gap increases, the conductivity decreases and subsequently the dielectric loss decreases (as shown in eqs 7 and 9).[54,65] It is to be noted that this rule may not be universally applicable in all the cases as exceptions do exist.[63] Moreover, unlike homogeneous material, these theories become even more complicated in the case of heterogeneous materials, such as polymer nanocomposites.

5. DO SEMICONDUCTING FILLERS HAVE THE POTENTIAL TO REPLACE THE CONVENTIONAL FILLERS?

Semiconducting fillers might stand as a potential candidate for EMI shielding applications. It depends primarily on electrical conductivity and the dielectric/magnetic properties of the material. It is observed that semiconductors with electrical conductivity near 1 S/m show reasonable EM absorption behavior. Many semiconductors such as ZnO, TiO_2, MoS_2, CoO, $BaTiO_3$, $SrTiO_3$, etc. are known to have good dielectric properties which play a crucial role in the losses, whereas there are a couple of semiconductors which have adequate magnetic properties (e.g., Fe_2O_3, Fe_3O_4, etc.), which aid in the EM absorption behavior. Hence, it is primarily the mechanism of shielding through the various types of losses (dipolar, interfacial, conduction, eddy current, magnetic) that decides whether a semiconducting material will prove to be a good shield for EM absorption. The mechanism of shielding is decided by the structure of each individual material/materials in the polymer matrix as well as their size and morphological features. Moreover, the mechanism is also governed by the interaction of these nanomaterials at various junctions, the state of aggregation, and the synergistic response of the polymer nanocomposite to the incoming EM radiations. Here, it is also worthwhile to note that there exist theories that correlate band gap to dielectric constant and dielectric loss. It is observed that with an increase in the band gap, both the dielectric constant and dielectric loss decrease. However, it may not be universally true for all semiconducting materials and at all frequencies. Moreover, for heterogeneous materials, such as polymer nanocomposites, these theories become even more complicated. To maximize the EM absorption properties, it is desirable to maximize tan δ_ε using a material with low dielectric constant and high dielectric loss. The other aspect to be noted is that the characteristic impedance of the absorber material ($z = (\mu/\varepsilon)^{1/2}$, valid for ideal dielectric) should be as close to the characteristic impedance of free space ($Z_0 = (\mu_0/\varepsilon_0)^{1/2} = 377\ \Omega$) in order to maximize EM absorption. If permittivity meets the EM impedance match requirement, a higher dielectric loss implies better EM absorption properties.[54]

Our survey of the existing literature shows that semiconducting fillers meet the commercial requirement of EMI shielding value of −20 dB and above, only at high loading percentage. It is to be noted that as the loading percentage of filler is increased, the mechanical aspect of the shield material is compromised. However, to exploit the absorption losses incurred due to the presence of semiconducting filler, a hybrid composite serves as a better alternative solution. For example, composites consisting of metallic or semiconductor particles

https://dx.doi.org/10.1021/acsomega.9b03641
ACS Omega 2020, 5, 4705−4718

embedded in a dielectric matrix have been widely explored in the literature.[60] The hybrid composite also enhances the number of interfaces and thus the dielectric mismatch which results in better shielding behavior.

AUTHOR INFORMATION

Corresponding Author

Suryasarathi Bose − *Department of Materials Engineering, Indian Institute of Science, Bangalore 560012, India;* orcid.org/0000-0001-8043-9192; Email: sbose@iisc.ac.in

Authors

Kumari Sushmita − *Centre for Nanoscience and Engineering, Indian Institute of Science, Bangalore 560012, India*

Giridhar Madras − *Interdisciplinary Centre for Energy Research, Indian Institute of Science, Bangalore 560012, India*

Complete contact information is available at: https://pubs.acs.org/10.1021/acsomega.9b03641

Notes

The authors declare no competing financial interest.

Biographies

Kumari Sushmita is currently a Ph.D. Researcher at Indian Institute of Science (IISc), Bangalore, India. Prior to joining IISc, she did her M.Tech in Chemical Engineering from the Indian Institute of Technology (IIT), Gandhinagar. In her M.Tech, she primarily worked on nanoparticle synthesis with its application in catalysis. Her current research interests include synthesis of hybrid structures, polymer nanocomposites, polymer blends, and designing multilayer stack-based assembly for EMI shielding applications.

Giridhar Madras is currently a Professor in the interdisciplinary department for energy research at the Indian Institute of Science (IISc), Bangalore, India. He obtained his M.Tech from Indian Institute of Technology (IIT), Madras, and Ph.D. in chemical engineering from Texas A&M University, USA. Afterward, he worked as a researcher at the University of California at Davis, USA. He is a recipient of the Shanti Swarup Bhatnagar Prize in 2009. He has made fundamental contributions in the area of catalysis, reactions in supercritical fluids, and polymer nanocomposites for various applications such as water remediation and EMI shielding.

Suryasarathi Bose is currently an Associate Professor in the department of materials engineering at the Indian Institute of Science (IISc), Bangalore, India. He received his M.Tech degree from the Institute of Chemical Technology (erstwhile UDCT), Mumbai, and a Ph.D. degree from the Indian Institute of Technology (IIT), Bombay. He then worked as a research associate at IIT Bombay before he joined Prof. Paula Moldenaers's group at Katholieke University of Leuven (Belgium) as a postdoctoral researcher. His research interests include polymer blends and nanocomposites, rheology, and structure−property correlations in homopolymers and blends, surface-initiated polymerization on nanoparticles and designing polymer-based materials for applications in EMI shielding and water filtration membranes.

ACKNOWLEDGMENTS

The authors would like to acknowledge the funding support from DST-SERB.

REFERENCES

(1) Sankaran, S.; Deshmukh, K.; Ahamed, M. B.; Khadheer Pasha, S. K. Recent advances in electromagnetic interference shielding properties of metal and carbon filler reinforced flexible polymer composites: A review. *Composites, Part A* **2018**, *114*, 49−71.

(2) Shahzad, F.; Alhabeb, M.; Hatter, C. B.; Anasori, B.; Man Hong, S.; Koo, C. M.; Gogotsi, Y. Electromagnetic interference shielding with 2D transition metal carbides (MXenes). *Science* **2016**, *353* (6304), 1137.

(3) Lin, K.-F.; Cheng, H.-M.; Hsu, H.-C.; Lin, L.-J.; Hsieh, W.-F. Band gap variation of size-controlled ZnO quantum dots synthesized by sol−gel method. *Chem. Phys. Lett.* **2005**, *409* (4), 208−211.

(4) Zhao, J.-Y.; Zhang, J.-M. Modulating the Band Gap of the FeS_2 by O and Se Doping. *J. Phys. Chem. C* **2017**, *121* (35), 19334−19340.

(5) Gorai, S.; Ganguli, D.; Chaudhuri, S. Synthesis of 1D Cu_2S with tailored morphology via single and mixed ionic surfactant templates. *Mater. Chem. Phys.* **2004**, *88* (2), 383−387.

(6) Heinemann, M.; Eifert, B.; Heiliger, C. Band structure and phase stability of the copper oxides Cu_2O, CuO, and Cu_4O_3. *Phys. Rev. B: Condens. Matter Mater. Phys.* **2013**, *87* (11), 115111.

(7) Yun, W. S.; Han, S. W.; Hong, S. C.; Kim, I. G.; Lee, J. D. Thickness and strain effects on electronic structures of transition metal dichalcogenides: 2H-MX_2 semiconductors (M = Mo, W; X = S, Se, Te). *Phys. Rev. B: Condens. Matter Mater. Phys.* **2012**, *85* (3), 033305.

(8) Cockayne, E.; Li, L. First-principles DFT+U studies of the atomic, electronic, and magnetic structure of α-MnO_2 (cryptomelane). *Chem. Phys. Lett.* **2012**, *544*, 53−58.

(9) Ninomiya, S.; Adachi, S. Optical properties of cubic and hexagonal CdSe. *J. Appl. Phys.* **1995**, *78* (7), 4681−4689.

(10) Nemade, K. R.; Waghuley, S. A. Band gap engineering of CuS nanoparticles for artificial photosynthesis. *Mater. Sci. Semicond. Process.* **2015**, *39*, 781−785.

(11) Wang, Y.; Ge, H. X.; Chen, Y. P.; Meng, X. Y.; Ghanbaja, J.; Horwat, D.; Pierson, J. F. Wurtzite CoO: a direct band gap oxide suitable for a photovoltaic absorber. *Chem. Commun.* **2018**, *54* (99), 13949−13952.

(12) Barakat, N. A. M.; Khil, M. S.; Sheikh, F. A.; Kim, H. Y. Synthesis and Optical Properties of Two Cobalt Oxides (CoO and Co_3O_4) Nanofibers Produced by Electrospinning Process. *J. Phys. Chem. C* **2008**, *112* (32), 12225−12233.

(13) Gusakova, J.; Wang, X.; Shiau, L. L.; Krivosheeva, A.; Shaposhnikov, V.; Borisenko, V.; Gusakov, V.; Tay, B. K. Electronic Properties of Bulk and Monolayer TMDs: Theoretical Study Within DFT Framework (GVJ-2e Method). *Phys. Status Solidi A* **2017**, *214* (12), 1700218.

(14) Valenzuela, M. A.; Bosch, P.; Jiménez-Becerrill, J.; Quiroz, O.; Páez, A. I. Preparation, characterization and photocatalytic activity of ZnO, Fe_2O_3 and $ZnFe_2O_4$. *J. Photochem. Photobiol., A* **2002**, *148* (1), 177−182.

(15) Bagbi, Y.; Sarswat, A.; Mohan, D.; Pandey, A.; Solanki, P. R. Lead and Chromium Adsorption from Water using L-Cysteine Functionalized Magnetite (Fe_3O_4) Nanoparticles. *Sci. Rep.* **2017**, *7* (1), 7672.

(16) Zelaya-Angel, O.; Alvarado-Gil, J. J.; Lozada-Morales, R.; Vargas, H.; Ferreira da Silva, A. Band-gap shift in CdS semiconductor by photoacoustic spectroscopy: Evidence of a cubic to hexagonal lattice transition. *Appl. Phys. Lett.* **1994**, *64* (3), 291−293.

(17) Bullett, D. W. The energy band structure of V_2O_5: a simpler theoretical approach. *J. Phys. C: Solid State Phys.* **1980**, *13* (23), L595−L599.

(18) Wang, F.; Di Valentin, C.; Pacchioni, G. Electronic and Structural Properties of WO_3: A Systematic Hybrid DFT Study. *J. Phys. Chem. C* **2011**, *115* (16), 8345−8353.

(19) Chithambararaj, A.; Bose, A. C. Hydrothermal synthesis of hexagonal and orthorhombic MoO_3 nanoparticles. *J. Alloys Compd.* **2011**, *509* (31), 8105−8110.

(20) Suzuki, K.; Kijima, K. Optical Band Gap of Barium Titanate Nanoparticles Prepared by RF-plasma Chemical Vapor Deposition. *Jpn. J. Appl. Phys.* **2005**, *44* (4A), 2081−2082.

(21) Dette, C.; Pérez-Osorio, M. A.; Kley, C. S.; Punke, P.; Patrick, C. E.; Jacobson, P.; Giustino, F.; Jung, S. J.; Kern, K. TiO_2 Anatase

with a Bandgap in the Visible Region. *Nano Lett.* **2014**, *14* (11), 6533−6538.
(22) van Benthem, K.; Elsasser, C.; French, R. H. Bulk electronic structure of $SrTiO_3$: Experiment and theory. *J. Appl. Phys.* **2001**, *90* (12), 6156−6164.
(23) Cheng, J.; Fan, D.; Wang, H.; Liu, B.; Zhang, Y.; Yan, H. Chemical bath deposition of crystalline ZnS thin films. *Semicond. Sci. Technol.* **2003**, *18* (7), 676−679.
(24) Parthibavarman, M.; Hariharan, V.; Sekar, C. High-sensitivity humidity sensor based on SnO_2 nanoparticles synthesized by microwave irradiation method. *Mater. Sci. Eng., C* **2011**, *31* (5), 840−844.
(25) Zhang, X.-J.; Li, S.; Wang, S.-W.; Yin, Z.-J.; Zhu, J.-Q.; Guo, A.-P.; Wang, G.-S.; Yin, P.-G.; Guo, L. Self-Supported Construction of Three-Dimensional MoS_2 Hierarchical Nanospheres with Tunable High-Performance Microwave Absorption in Broadband. *J. Phys. Chem. C* **2016**, *120* (38), 22019−22027.
(26) Menon, A. V.; Madras, G.; Bose, S. Mussel-Inspired Self-Healing Polyurethane with "Flower-like" Magnetic MoS_2 as Efficient Microwave Absorbers. *ACS Appl. Polym. Mater.* **2019**, *1*, 2417.
(27) Wang, Y.; Chen, D.; Yin, X.; Xu, P.; Wu, F.; He, M. Hybrid of MoS_2 and Reduced Graphene Oxide: A Lightweight and Broadband Electromagnetic Wave Absorber. *ACS Appl. Mater. Interfaces* **2015**, *7* (47), 26226−26234.
(28) Ding, X.; Huang, Y.; Li, S.; Zhang, N.; Wang, J. 3D architecture reduced graphene oxide-MoS_2 composite: Preparation and excellent electromagnetic wave absorption performance. *Composites, Part A* **2016**, *90*, 424−432.
(29) Ran, J.; Shen, L.; Zhong, L.; Fu, H. Synthesis of Silanized MoS_2/Reduced Graphene Oxide for Strong Radar Wave Absorption. *Ind. Eng. Chem. Res.* **2017**, *56* (38), 10667−10677.
(30) Zhou, M.; Zhang, X.; Wei, J.; Zhao, S.; Wang, L.; Feng, B. Morphology-Controlled Synthesis and Novel Microwave Absorption Properties of Hollow Urchinlike α-MnO_2 Nanostructures. *J. Phys. Chem. C* **2011**, *115* (5), 1398−1402.
(31) Bora, P. J.; Vinoy, K. J.; Ramamurthy, P. C.; Madras, G. Electromagnetic interference shielding efficiency of MnO_2 nanorod doped polyaniline film. *Mater. Res. Express* **2017**, *4* (2), 025013.
(32) Cao, M.; Lian, H.; Hu, C. Ligand-assisted fabrication of hollow CdSe nanospheres via Ostwald ripening and their microwave absorption properties. *Nanoscale* **2010**, *2* (12), 2619−2623.
(33) He, S.; Wang, G.-S.; Lu, C.; Luo, X.; Wen, B.; Guo, L.; Cao, M.-S. Controllable Fabrication of CuS Hierarchical Nanostructures and Their Optical, Photocatalytic, and Wave Absorption Properties. *ChemPlusChem* **2013**, *78* (3), 250−258.
(34) Hu, X.-S.; Shen, Y.; Xu, L.-H.; Wang, L.-M.; Lu, L.-s.; Zhang, Y.-t. Preparation of flower-like CuS by solvothermal method for photocatalytic, UV protection and EMI shielding applications. *Appl. Surf. Sci.* **2016**, *385*, 162−170.
(35) Hu, X.-S.; Shen, Y. Fabrication of novel polyaniline/flowerlike copper monosulfide composites with enhanced electromagnetic interference shielding effectiveness. *J. Appl. Polym. Sci.* **2017**, *134* (34), 45232.
(36) Liu, P.; Huang, Y.; Yan, J.; Yang, Y.; Zhao, Y. Construction of CuS Nanoflakes Vertically Aligned on Magnetically Decorated Graphene and Their Enhanced Microwave Absorption Properties. *ACS Appl. Mater. Interfaces* **2016**, *8* (8), 5536−5546.
(37) Sun, G.; Zhang, X.; Cao, M.; Wei, B.; Hu, C. Facile Synthesis, Characterization, and Microwave Absorbability of CoO Nanobelts and Submicrometer Spheres. *J. Phys. Chem. C* **2009**, *113* (17), 6948−6954.
(38) Zhang, D.-Q.; Liu, T.-T.; Shu, J.-C.; Liang, S.; Wang, X.-X.; Cheng, J.-Y.; Wang, H.; Cao, M.-S. Self-Assembly Construction of WS_2−rGO Architecture with Green EMI Shielding. *ACS Appl. Mater. Interfaces* **2019**, *11* (30), 26807−26816.
(39) Lu, M.; Wang, X.; Cao, W.; Yuan, J.; Cao, M. Carbon nanotube-CdS core-shell nanowires with tunable and high-efficiency microwave absorption at elevated temperature. *Nanotechnology* **2016**, *27* (6), 065702.
(40) Sastry, D. N.; Revanasiddappa, M.; Suresh, T.; Kiran, Y. T. R.; Raghavendra, S. C. Electromagnetic shielding effectiveness studies on polyaniline/CSA-WO_3 composites at KU band frequencies. *AIP Conf. Proc.* **2017**, *1953* (1), 090067.
(41) Boujar Dolabi, M.; Azimi, A.; Hossein Hosseini, S. Preparation of thermal infrared and microwave absorber using WO_3/$MnFe_3O_4$/polyaniline nanocomposites. *Mater. Res. Innovations* **2019**, 1−9.
(42) Wang, Y.; Wu, X.; Zhang, W.; Luo, C.; Li, J.; Wang, Q. 3D heterostructure of graphene@Fe_3O_4@WO_3@PANI: Preparation and excellent microwave absorption performance. *Synth. Met.* **2017**, *231*, 7−14.
(43) Lyu, L.; Wang, F.; Qiao, J.; Ding, X.; Zhang, X.; Xu, D.; Liu, W.; Liu, J. Novel synthesis of MoO_3/Mo_4O_{11}/MoO_2 heterogeneous nanobelts for wideband electromagnetic wave absorption. *J. Alloys Compd.* **2020**, *817*, 153309.
(44) Li, C.-Q.; Shen, X.; Ding, R.-C.; Wang, G.-S. Controllable Synthesis of One-Dimensional MoO_3/MoS_2 Hybrid Composites with their Enhanced Efficient Electromagnetic Wave Absorption Properties. *ChemPlusChem* **2019**, *84* (2), 226−232.
(45) Zhu, Y.-F.; Zhang, L.; Natsuki, T.; Fu, Y.-Q.; Ni, Q.-Q. Facile Synthesis of $BaTiO_3$ Nanotubes and Their Microwave Absorption Properties. *ACS Appl. Mater. Interfaces* **2012**, *4* (4), 2101−2106.
(46) Chauhan, S. S.; Verma, P.; Malik, R. S.; Choudhary, V. Thermomechanically stable dielectric composites based on poly(ether ketone) and $BaTiO_3$ with improved electromagnetic shielding properties in X-band. *J. Appl. Polym. Sci.* **2018**, *135* (26), 46413.
(47) Abbas, S. M.; Dixit, A. K.; Chatterjee, R.; Goel, T. C. Complex permittivity and microwave absorption properties of $BaTiO_3$−polyaniline composite. *Mater. Sci. Eng., B* **2005**, *123* (2), 167−171.
(48) Guo, A.-P.; Zhang, X.-J.; Qu, J.-K.; Wang, S.-W.; Zhu, J.-Q.; Wang, G.-S.; Guo, L. Improved microwave absorption and electromagnetic interference shielding properties based on graphene−barium titanate and polyvinylidene fluoride with varying content. *Mater. Chem. Front.* **2017**, *1* (12), 2519−2526.
(49) Zhuo, R. F.; Feng, H. T.; Chen, J. T.; Yan, D.; Feng, J. J.; Li, H. J.; Geng, B. S.; Cheng, S.; Xu, X. Y.; Yan, P. X. Multistep Synthesis, Growth Mechanism, Optical, and Microwave Absorption Properties of ZnO Dendritic Nanostructures. *J. Phys. Chem. C* **2008**, *112* (31), 11767−11775.
(50) Singh, R.; Kulkarni, S. G. Nanocomposites based on transition metal oxides in polyvinyl alcohol for EMI shielding application. *Polym. Bull.* **2014**, *71* (2), 497−513.
(51) Phang, S. W.; Tadokoro, M.; Watanabe, J.; Kuramoto, N. Microwave absorption behaviors of polyaniline nanocomposites containing TiO_2 nanoparticles. *Curr. Appl. Phys.* **2008**, *8* (3), 391−394.
(52) Dhawan, S. K.; Singh, K.; Bakhshi, A. K.; Ohlan, A. Conducting polymer embedded with nanoferrite and titanium dioxide nanoparticles for microwave absorption. *Synth. Met.* **2009**, *159* (21), 2259−2262.
(53) Akman, O.; Durmus, Z.; Kavas, H.; Aktas, B.; Kurtan, U.; Baykal, A.; Sözeri, H. Effect of conducting polymer layer on microwave absorption properties of $BaFe_{12}O_{19}$-TiO_2 composite. *Phys. Status Solidi A* **2013**, *210* (2), 395−402.
(54) Kong, L.; Yin, X.; Ye, F.; Li, Q.; Zhang, L.; Cheng, L. Electromagnetic Wave Absorption Properties of ZnO-Based Materials Modified with $ZnAl_2O_4$ Nanograins. *J. Phys. Chem. C* **2013**, *117* (5), 2135−2146.
(55) Song, W.-L.; Cao, M.-S.; Wen, B.; Hou, Z.-L.; Cheng, J.; Yuan, J. Synthesis of zinc oxide particles coated multiwalled carbon nanotubes: Dielectric properties, electromagnetic interference shielding and microwave absorption. *Mater. Res. Bull.* **2012**, *47* (7), 1747−1754.
(56) Han, M.; Yin, X.; Ren, S.; Duan, W.; Zhang, L.; Cheng, L. Core/shell structured C/ZnO nanoparticles composites for effective electromagnetic wave absorption. *RSC Adv.* **2016**, *6* (8), 6467−6474.
(57) Wu, F.; Xia, Y.; Wang, Y.; Wang, M. Two-step reduction of self-assembled three-dimensional (3D) reduced graphene oxide (RGO)/

https://dx.doi.org/10.1021/acsomega.9b03641
ACS Omega 2020, 5, 4705−4718

zinc oxide (ZnO) nanocomposites for electromagnetic absorption. *J. Mater. Chem. A* **2014**, *2* (47), 20307−20315.
(58) Murugan, M.; Bapat, M. S.; Kokate, V. K. Composites of nanosized strontium titanate epoxy resin as microwave absorber. *Journal of Electromagnetic Waves and Applications* **2016**, *30* (3), 366−374.
(59) Choi, H. D.; Shim, H. W.; Cho, K. Y.; Lee, H. J.; Park, C. S.; Yoon, H. G. Electromagnetic and electromagnetic wave-absorbing properties of the $SrTiO_3$−Epoxy composite. *J. Appl. Polym. Sci.* **1999**, *72* (1), 75−83.
(60) Feng, H.; Zhuo, R.; Chen, J.; Yan, D.; Feng, J.; Li, H.; Cheng, S.; Wu, Z.; Wang, J.; Yan, P. Synthesis, Characterization, and Microwave Absorption Property of the SnO_2 Nanowire/Paraffin Composites. *Nanoscale Res. Lett.* **2009**, *4* (12), 1452.
(61) Zhao, B.; Fan, B.; Xu, Y.; Shao, G.; Wang, X.; Zhao, W.; Zhang, R. Preparation of Honeycomb SnO_2 Foams and Configuration-Dependent Microwave Absorption Features. *ACS Appl. Mater. Interfaces* **2015**, *7* (47), 26217−26225.
(62) Liu, J.; Cheng, J.; Che, R.; Xu, J.; Liu, M.; Liu, Z. Double-Shelled Yolk−Shell Microspheres with Fe_3O_4 Cores and SnO_2 Double Shells as High-Performance Microwave Absorbers. *J. Phys. Chem. C* **2013**, *117* (1), 489−495.
(63) Yim, K.; Yong, Y.; Lee, J.; Lee, K.; Nahm, H.-H.; Yoo, J.; Lee, C.; Seong Hwang, C.; Han, S. Novel high-κ dielectrics for next-generation electronic devices screened by automated ab initio calculations. *NPG Asia Mater.* **2015**, *7* (6), e190−e190.
(64) Sun, C. Q.; Sun, X. W.; Tay, B. K.; Lau, S. P.; Huang, H. T.; Li, S. Dielectric suppression and its effect on photoabsorption of nanometric semiconductors. *J. Phys. D: Appl. Phys.* **2001**, *34* (15), 2359−2362.
(65) Sati, A.; Kumar, A.; Mishra, V.; Warshi, K.; Sagdeo, A.; Anwar, S.; Kumar, R.; Sagdeo, P. R. Direct correlation between the band gap and dielectric loss in Hf doped $BaTiO_3$. *J. Mater. Sci.: Mater. Electron.* **2019**, *30* (8), 8064−8070.
(66) Kittel, C. *Introduction to Solid State Physics*, 8th ed.; Wiley, 1956; pp 393−401.

https://dx.doi.org/10.1021/acsomega.9b03641
ACS Omega 2020, 5, 4705−4718